Inorganic Chemistry

Article

pubs.acs.org/IC

Investigation of the Energy-Transfer Mechanism in Ho^{3+}- and Yb^{3+}-Codoped Lu_2O_3 Phosphor with Efficient Near-Infrared Downconversion

Guotao Xiang,*[,†] Yan Ma,[†] Xianju Zhou,[†] Sha Jiang,[†] Li Li,[†] Xiaobing Luo,[†] Zhendong Hao,[‡] Xia Zhang,[‡] Guo-Hui Pan,[‡] Yongshi Luo,[‡] and Jiahua Zhang*[,‡]

[†]Department of Mathematics and Physics, Chongqing University of Posts and Telecommunications, 2 Chongwen Road, Chongqing 400065, China

[‡]State Key Laboratory of Luminescence and Applications, Changchun Institute of Optics, Fine Mechanics and Physics, Chinese Academy of Sciences, 3888 Eastern South Lake Road, Changchun 130033, China

ABSTRACT: A high-temperature solid-state method was used to synthesize the Ho^{3+}- and Yb^{3+}-codoped cubic Lu_2O_3 powders. The crystal structures of the as-prepared powders were characterized by X-ray diffraction. The energy-transfer (ET) phenomenon between Ho^{3+} ions and Yb^{3+} ions was verified by the steady-state spectra including visible and near-infrared (NIR) regions. Beyond that, the decay curves were also measured to certify the existence of the ET process. The downconversion phenomena appeared when the samples were excited by 446 nm wavelength corresponding to the transition of Ho^{3+}: $^5I_8 \rightarrow {}^5G_6/{}^5F_1$. On the basis of the analysis of the relationship between the initial transfer rate of Ho^{3+}: $^5F_3$ level and the Yb^{3+} doping concentration, it indicates that the ET from $^5F_3$ state of Ho^{3+} ions to $^2F_{5/2}$ state of Yb^{3+} ions is mainly through a two-step ET process, not the long-accepted cooperative ET process. In addition, a 62% ET efficiency can be achieved in Lu_2O_3: 1% Ho^{3+}/30% Yb^{3+}. Unlike the common situations in which the NIR photons are all emitted by the acceptors Yb^{3+}, the sensitizers Ho^{3+} also make contributions to the NIR emission upon 446 nm wavelength excitation. Meanwhile, the $^5I_5 \rightarrow {}^5I_8$ transition and $^5F_4/{}^5S_2 \rightarrow {}^5I_6$ transition of Ho^{3+} as well as the $^2F_{5/2} \rightarrow {}^2F_{7/2}$ transition of Yb^{3+} match well with the optimal spectral response of crystalline silicon solar cells. The current research indicates that Lu_2O_3: Ho^{3+}/Yb^{3+} is a promising material to improve conversion efficiency of crystalline silicon solar cell.

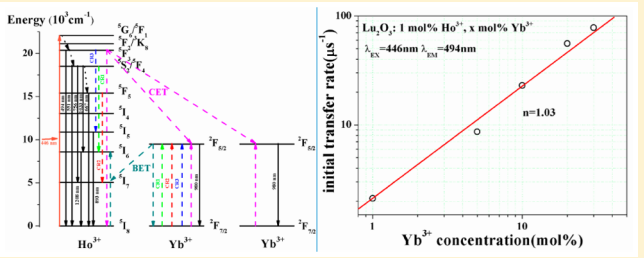

INTRODUCTION

Nowadays, trivalent lanthanide ions doped phosphors have attracted great interest due to their new features and versatile applicability.[1−3] Trivalent lanthanide ions could not only exhibit upconversion (UC) properties but also own down-conversion (DC) emissions, manifesting as dividing one high-energy photon into two or more lower-energy photons. Thanks to such a unique character, DC materials can be widely applied in nonmercury lamp, solid-state laser, plasma display technology, and so on.[4−6] Especially in improving the solar cell efficiency, near-infrared (NIR) DC is considered as a promising method.[7,8] As is well-known, the maximum efficiency of the commercial crystalline silicon solar cell is only 18% because of the spectrum mismatch between the solar spectrum (300 nm −2500 nm) and the response spectrum of crystalline silicon solar cell (500−1100 nm).[9−14] Thus, the photons with the wavelengths shorter than 500 nm are unavailable for the silicon solar cell, even though the solar radiation is very strong in the region from 300 to 500 nm. Fortunately, sunlight shorter than 500 nm can be transformed into NIR light, which can be utilized by crystalline silicon solar cell through a NIR DC process, so that the efficiency improvement of the crystalline silicon solar cell can be realized. As reported by T. Trupke et al., utilizing the suitable DC material, the actual efficiency of the silicon solar cells can be increased up to 39.63%, largely exceeding the maximum energy efficiency 30% estimated by Shockley and Queisser.[15,16]

Lu_2O_3 has been proved to be an excellent host for trivalent lanthanide ions doping, even at high doping concentration.[17] Moreover, Lu_2O_3 exhibits good thermal stability, insulating property, hygroscopic immunity, and environmentally friendly characteristics.[18] These properties make Lu_2O_3 suitable for practical application. More importantly, Lu_2O_3 has a low phonon energy of ∼600 cm^{-1}, which can suppress the nonradiative relaxation during the DC process resulting in high DC quantum yield.[19] The properties mentioned above indicate that Lu_2O_3 is an excellent host for DC. For the activator of NIR DC process, Yb^{3+} ion, is the most widely used because of its high emission quantum efficiency at ∼1 μm just above the band edge of crystalline silicon. Ho^{3+} ion has suitable energy levels that match well with Yb^{3+} ion and favorable

Received: October 26, 2016
Published: January 18, 2017

DOI: 10.1021/acs.inorgchem.6b02600
Inorg. Chem. 2017, 56, 1498−1503

metastable energy levels for DC emission, so Ho^{3+} ion and Yb^{3+} ion are a good combination in NIR DC investigation. In recent years, large efforts have been devoted to the study of the DC emission realized with Ho^{3+}/Yb^{3+} couple in a variety of hosts.[20−23] However, the DC properties in Ho^{3+}- and Yb^{3+}-codoped Lu_2O_3 host are rarely studied. Beyond that, under the excitation of $^5G_6/^5F_1$ or higher energy level of Ho^{3+}, cooperative energy-transfer (ET) process is considered as the main route for the ET from $^5F_3$ level of Ho^{3+} ions to $^2F_{5/2}$ level of Yb^{3+} ions. But, as far as we know, this long-accepted mechanism is proposed only based on theory and lack of effective experimental data supporting this phenomenon adequately.

In this paper, an efficient NIR DC process was demonstrated in Ho^{3+}- and Yb^{3+}-codoped Lu_2O_3. The dependences of Yb^{3+} concentration on the steady-state spectra including visible and NIR regions, decay curves, as well as ET efficiency were discussed. The ET mechanisms during the DC process were explored with the dependence of the initial transfer rate on Yb^{3+} ion concentration. Results show Ho^{3+}- and Yb^{3+}-codoped Lu_2O_3 phosphor is an excellent DC material and fit for the application of solar cells.

EXPERIMENTAL SECTION

Chemicals. Lu_2O_3, Ho_2O_3, and Yb_2O_3 with spectroscopic pure grade (99.99%) were supplied by Yang Kou state run rare-earth company. The powders were all used as obtained without any purification.

Preparation of Lu_2O_3: 1 mol % Ho^{3+}/x mol % Yb^{3+} (x = 0, 1, 5, 10, 20, 30). The Lu_2O_3: 1 mol % Ho^{3+}/x mol % Yb^{3+} powder were synthesized by a solid-state reaction. The Lu_2O_3, Ho_2O_3, and Yb_2O_3 were used as the raw materials, which were mixed homogeneously by an agate mortar for 1.5 h, placed in an alumina crucible with a lid, then sintered in a box furnace at 1550 °C for 5 h in air.

Characterization. Powder X-ray diffraction (XRD) data of the as-prepared samples were detected using Cu Kα radiation (λ = 1.540 56 Å) on a Bruker D8 advance diffractometer. An FLS920 spectrometer purchased from Edinburgh Instruments was employed to measure the excitation and emission spectra. The decay curves were collected through a Tektronix digital oscilloscope (TDS 3052) with an optical parametric oscillator as the excitation source.

RESULTS AND DISCUSSION

Structure. The XRD patterns of Lu_2O_3: 1% Ho^{3+}/x% Yb^{3+} synthesized by the high-temperature solid-state method were shown in Figure 1. As can be seen obviously, the positions and relative intensity of the diffraction peaks for the as-prepared products match well with the standard cards of the cubic Lu_2O_3 (JCPDS No. 43−1021) with space group $Ia3$ (No. 206). No impurity phase is observed in XRD patterns, demonstrating Ho^{3+} and Yb^{3+} are all incorporated into Lu_2O_3 and formed a solid solution structure. In addition, as the difference between radius of Lu^{3+} (1.117 Å) and Yb^{3+} (1.125 Å) is very small, the XRD diffraction peaks did not show obvious shift with the increasing Yb^{3+} concentration, even though at 30 mol % doping concentration of Yb^{3+}.

Luminescence Properties. A batch of powders with 1 mol % Ho^{3+} doping concentration and different Yb^{3+} doping concentrations (0, 1, 5, 10, 20, and 30 mol %) were synthesized for the investigation of the NIR DC mechanism in Ho^{3+} and Yb^{3+} pairs. As shown in Figures 2−5, the fluorescence excitation and emission spectra of the prepared products were utilized to prove the existence of $Ho^{3+}\rightarrow Yb^{3+}$ ET first. Observe the excitation spectra of Ho^{3+}: $^5F_4/^5S_2\rightarrow{}^5I_8$ at 551 nm and $^5F_5\rightarrow{}^5I_8$

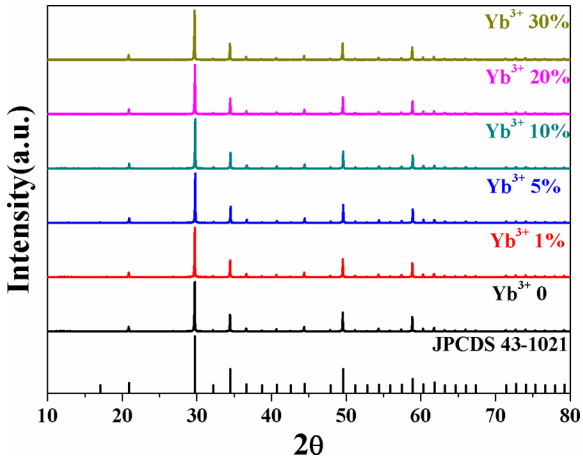

Figure 1. XRD patterns of Lu_2O_3: 1% Ho^{3+}/x% Yb^{3+} with the standard XRD data of cubic Lu_2O_3 (JCPDS No. 43−1021).

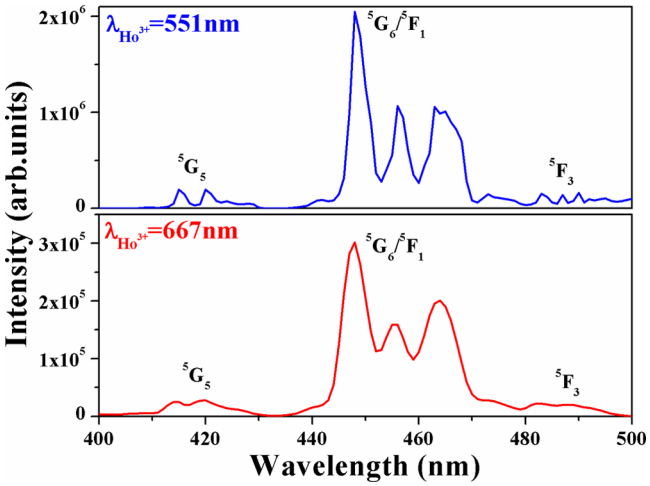

Figure 2. Excitation spectra of Ho^{3+}: $^5F_4/^5S_2\rightarrow{}^5I_8$ emission (551 nm, blue line) and Ho^{3+}: $^5F_5\rightarrow{}^5I_8$ emission (667 nm, red line) in Lu_2O_3: 1 mol % Ho^{3+}/5 mol % Yb^{3+} powder sample.

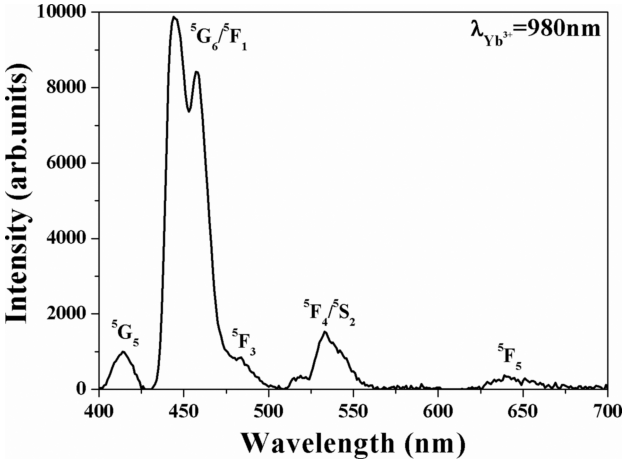

Figure 3. Excitation spectra of Yb^{3+}: $^2F_{5/2}\rightarrow{}^2F_{7/2}$ transition (980 nm) in Lu_2O_3: 1 mol % Ho^{3+}/5 mol % Yb^{3+} powder sample.

at 667 nm; both of them exhibit three distinct absorption peaks located at 420, 446, and 494 nm, which belong to Ho^{3+}: $^5I_8\rightarrow{}^5G_5$, $^5I_8\rightarrow{}^5G_6/^5F_1$, and $^5I_8\rightarrow{}^5F_3$, respectively. In the meantime, the three absorption peaks also appear in the

DOI: 10.1021/acs.inorgchem.6b02600
Inorg. Chem. 2017, 56, 1498−1503

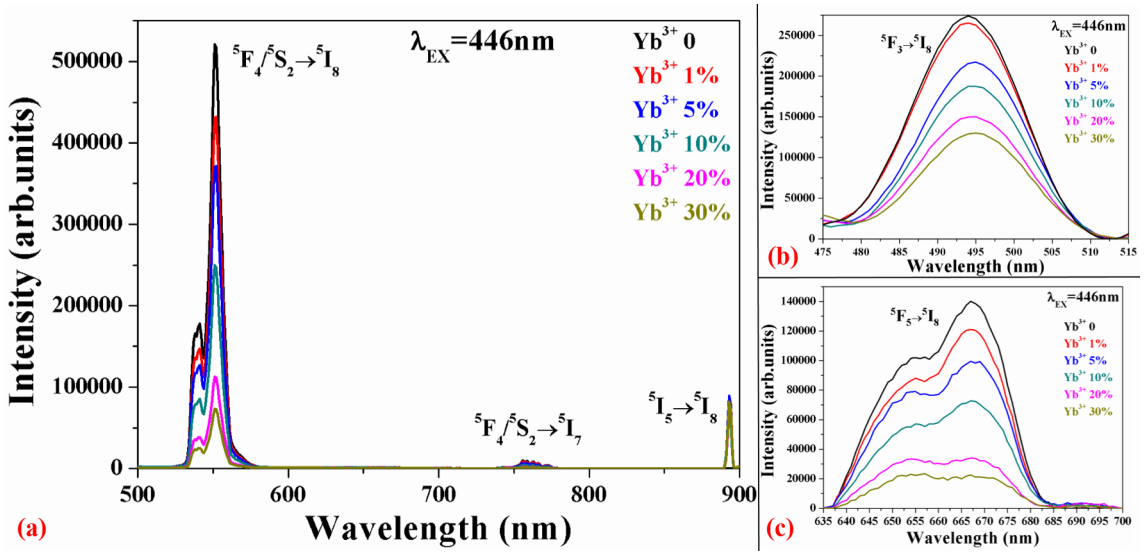

Figure 4. Visible emission spectra in the range of (a) 500−900 nm, (b) 475−515 nm, and (c) 635−700 nm in Lu_2O_3: 1% Ho^{3+}/*x*% Yb^{3+} under 446 nm excitation.

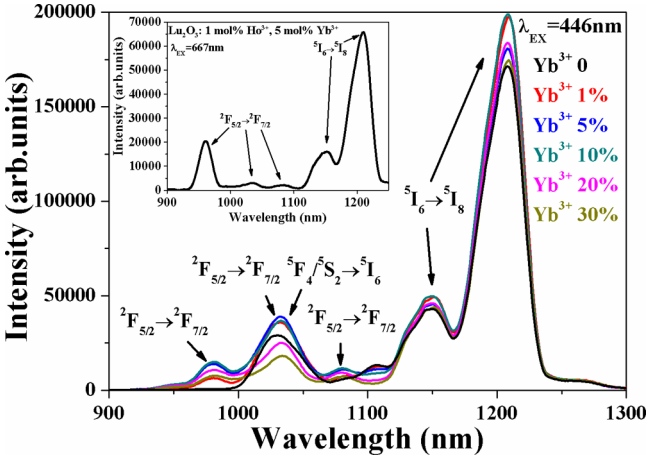

Figure 5. NIR emission spectra of Lu_2O_3: 1% Ho^{3+}/*x*% Yb^{3+} under 446 nm excitation. (inset) NIR emission spectrum in Lu_2O_3: 1 mol % Ho^{3+}/5 mol % Yb^{3+} under 667 nm excitation.

excitation spectrum of Yb^{3+}: $^2F_{5/2}\rightarrow{}^2F_{7/2}$ infrared emission at 980 nm shown in Figure 3, which manifest the existence of ET from Ho^{3+} to Yb^{3+}. Besides, as can be seen from Figure 3, the excitation spectrum for monitoring Yb^{3+}: $^2F_{5/2}\rightarrow{}^2F_{7/2}$ transition includes two extra excitation bands in the range of 500−700 nm, which belong to Ho^{3+}: $^5I_8\rightarrow{}^5F_4/{}^5S_2$ and $^5I_8\rightarrow{}^5F_5$, respectively, demonstrating $^5F_4/{}^5S_2$ level and $^5F_5$ level of Ho^{3+} can also transfer energy toYb^{3+}.

The visible and NIR emission spectra are measured by 446 nm excitation, which is attributed to the absorption of Ho^{3+}: $^5I_8\rightarrow{}^5G_6/{}^5F_1$. As shown in Figure 4a, the spectra display two evident emission bands located at ∼551 and 756 nm in the range of 500−800 nm, which belong to the $^5F_4/{}^5S_2\rightarrow{}^5I_8$ transition and $^5F_4/{}^5S_2\rightarrow{}^5I_7$ transition of Ho^{3+}, respectively. Furthermore, there are two weak emissions existing in the ranges of 475−510 nm and 635−700 nm shown in Figure 4b,c, which are attributed to $^5F_3\rightarrow{}^5I_8$ transition and $^5F_5\rightarrow{}^5I_8$ transition of Ho^{3+}, respectively. Besides, an emission peak around 893 nm derived from $^5I_5\rightarrow{}^5I_8$ transition of Ho^{3+} appears in Ho^{3+}- and Yb^{3+}-codoped samples. Figure 5 shows the NIR region spectra of the as-prepared powders excited by 446 nm wavelength. The Ho^{3+} singly doped and Ho^{3+}/Yb^{3+}-codoped samples exhibit a strong emission band peaked at ∼1208 nm, which is assigned to Ho^{3+}: $^5I_6\rightarrow{}^5I_8$ transition. As for the Ho^{3+} singly doped sample, the emission peak located at 1033 nm is attributed to $^5F_4/{}^5S_2\rightarrow{}^5I_6$ transition of Ho^{3+}. In the Ho^{3+}- and Yb^{3+}-codoped samples, the $^2F_{5/2}\rightarrow{}^2F_{7/2}$ transition of Yb^{3+} appears extending from 900 to 1100 nm. In this range, it is easily to observe two distinct emission peaks around 980 and 1080 nm, which belong to $^2F_{5/2}\rightarrow{}^2F_{7/2}$ transition of Yb^{3+}. The phenomenon that the NIR emission of Yb^{3+} is exhibited under the direct excitation of the $^5G_6/{}^5F_1$ level of Ho^{3+} is another evidence for ET from Ho^{3+} to Yb^{3+}. Here, it is necessary to point out that, except for the $^5F_4/{}^5S_2\rightarrow{}^5I_6$ transition of Ho^{3+}, the $^2F_{5/2}\rightarrow{}^2F_{7/2}$ transition of Yb^{3+} also devotes to the emission peak around 1033 nm in the Ho^{3+}- and Yb^{3+}-codoped samples. This can be explained by the NIR spectra of the codoped samples excited by 667 nm wavelength. In the spectra measurement, 667 nm is selected to excite the $^5F_5$ level of Ho^{3+}, so that it can be avoid to excite $^5F_4/{}^5S_2$ level of Ho^{3+}. As shown in the inset of Figure 5, from the range of 900−1100 nm, the three emission peaks located at 980, 1033, and 1080 nm should be all assigned to the $^2F_{5/2}\rightarrow{}^2F_{7/2}$ transition of Yb^{3+}, resulting from the Stark splitting of $^2F_{5/2}$ state and $^2F_{7/2}$ state.[24] That is to say, the emission intensity of the peak located at 1033 nm is jointly contributed by the $^5F_4/{}^5S_2\rightarrow{}^5I_6$ transition of Ho^{3+} and the $^2F_{5/2}\rightarrow{}^2F_{7/2}$ transition of Yb^{3+} in Ho^{3+}- and Yb^{3+}-codoped samples.

It can be seen clearly that the intensity of $^5F_3\rightarrow{}^5I_8$ transition, $^5F_4/{}^5S_2\rightarrow{}^5I_8$ transition, $^5F_5\rightarrow{}^5I_8$ transition, and $^5F_4/{}^5S_2\rightarrow{}^5I_7$ transition of Ho^{3+} is reduced dramatically with the increased Yb^{3+} ion concentration. Moreover, the intensity of the $^2F_{5/2}\rightarrow{}^2F_{7/2}$ transition of Yb^{3+} is enhanced along with increasing Yb^{3+} doping concentration up to 10 mol %. This phenomenon demonstrates once again the $Ho^{3+}\rightarrow Yb^{3+}$ ET. The concentration quenching occurs when Yb^{3+} concentration reaches 20 mol %, indicating the optimal doped concentration of Yb^{3+} is 10 mol % with 1 mol % Ho^{3+}. In addition, since the $^5I_6$ state of Ho^{3+} is slightly lower than $^2F_{5/2}$ state of Yb^{3+}, the excited Yb^{3+} can transfer its energy back to $^5I_6$ state of Ho^{3+}

DOI: 10.1021/acs.inorgchem.6b02600
Inorg. Chem. 2017, 56, 1498−1503

easily, which has been proved clearly by Wang's group.[21] Therefore, the $^5I_6 \rightarrow {}^5I_8$ transition of Ho^{3+} can be enhanced by this energy back transfer (BET) process, and the $^2F_{5/2} \rightarrow {}^2F_{7/2}$ transition of Yb^{3+} is reduced at the same time.

To understand the DC mechanism in Ho^{3+}- and Yb^{3+}-codoped system in depth, the possible ET routes are presented in Figure 6. Excited by 446 nm wavelength, Ho^{3+} ion in the

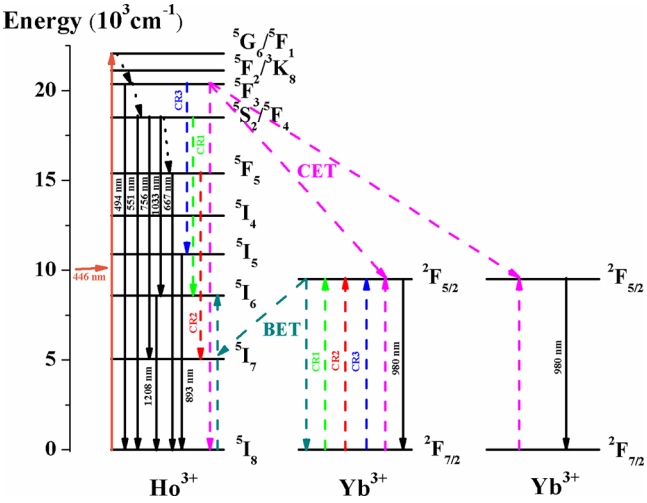

Figure 6. Energy-level diagram and possible ET routes in Lu_2O_3: Ho^{3+}/Yb^{3+}.

ground state $^5I_8$ is excited to $^5G_6/^5F_1$ state. Subsequently, $^5F_3$ level, $^5F_4/^5S_2$ level, and $^5F_5$ level can be populated by nonradiative relaxation processes from the corresponding upper state. Then, the Ho^{3+} in $^5F_4/^5S_2$ or $^5F_5$ state can transfer its energy to one nearby Yb^{3+} through cross-relaxation processes CR1 and CR2, respectively.[25] Specially, the Ho^{3+}: $^5I_8 \rightarrow {}^5F_3$ transition is located at approximately twice the energy of the Yb^{3+}: $^2F_{5/2} \rightarrow {}^2F_{7/2}$ transition, and the position of $^5I_5$ state of Ho^{3+} is a little higher than that of $^2F_{5/2}$ state of Yb^{3+}. In addition, Yb^{3+} has no other levels up to the UV region. Therefore, the ET from Ho^{3+} in $^5F_3$ level to Yb^{3+} has two possible routes: (a) two-step ET, as shown in Figure 6: the first ET step is that the Ho^{3+} ion in $^5F_3$ level transfers its energy to one Yb^{3+} ion through CR3 [$^5F_3$ (Ho^{3+}) + $^2F_{7/2}$ (Yb^{3+}) $\rightarrow {}^5I_5$ (Ho^{3+}) + $^2F_{5/2}$ (Yb^{3+})]; next, the second ET step is that the Ho^{3+} ion in $^5I_5$ level is de-excited to the ground state and then transfers its energy to another Yb^{3+} ion [$^5I_5$ (Ho^{3+}) + $^2F_{7/2}$ (Yb^{3+}) $\rightarrow {}^5I_8$ (Ho^{3+}) + $^2F_{5/2}$ (Yb^{3+})]. (b) Cooperative ET (CET), as shown in Figure 6: two Yb^{3+} ions in the ground state are simultaneously excited to $^2F_{5/2}$ state by receiving energy from the same Ho^{3+} ion in $^5F_3$ level.

According to our previous report, assuming the ET from Ho^{3+} in $^5F_3$ level to Yb^{3+} is mainly through a two-step ET process, the initial ET rate W_{CR} should be proportional to the acceptor concentration x, which can be taken as $W_{CR} \propto x$; if the CET process is dominant in the ET from Ho^{3+} in $^5F_3$ level to Yb^{3+}, the initial ET rate W_{COOP} should be proportional to the square of the acceptor concentration, which can be written as $W_{COOP} \propto x^2$.[8]

On the basis of the principle mentioned above, we need to explore the relationship between the initial transfer rate and Yb^{3+} ion concentration to judge the ET mechanism from $^5F_3$ level of Ho^{3+} ions to Yb^{3+} ions. Figure 7 shows the decay curves of Ho^{3+}: $^5F_3$ level in the as-prepared Lu_2O_3: 1% Ho^{3+}/x% Yb^{3+}

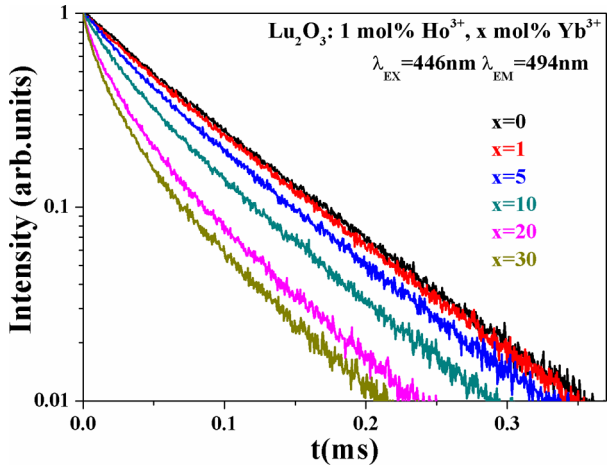

Figure 7. Decay curves of Ho^{3+}: $^5F_3$ level in Lu_2O_3: 1 mol % Ho^{3+}/x mol % Yb^{3+}. (λ_{EX} = 446 nm, λ_{EM} = 494 nm).

(x = 0, 1, 5, 10, 20, 30). Choosing the curves from the beginning to 70% of the maximum intensity as the targets, the initial decay rate $W_{Yb(x\%)}$ of samples can be achieved from their slopes. Subsequently, the initial transfer rate of each sample can be calculated by

$$W_{Ho-Yb(x\%)} = W_{Yb(x\%)} - W_{Yb(0)} \quad (1)$$

Consequently, the relationship between the initial transfer rate and Yb^{3+} ion concentration is obtained and presented in Figure 8. As can be seen clearly, the n value is 1.03 with

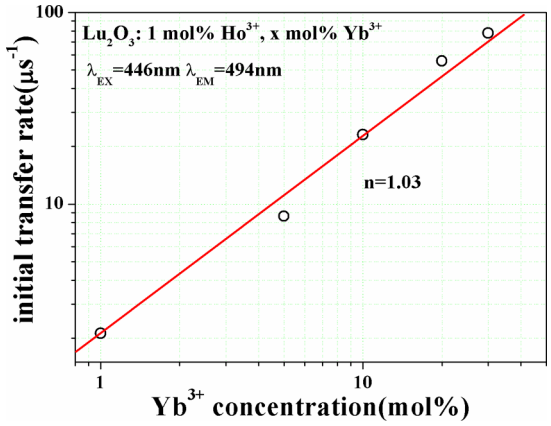

Figure 8. Double-logarithmic plots of Yb^{3+} doping concentration dependent on the initial transfer rate in Lu_2O_3: 1 mol % Ho^{3+}/x mol % Yb^{3+}.

increasing Yb^{3+} ion doping concentration from 1 to 30 mol %, demonstrating the ET from $^5F_3$ level of Ho^{3+} to $^2F_{5/2}$ level of Yb^{3+} is mainly through the two-step ET process. Moreover, as shown in Figure 4a, the $^5I_5 \rightarrow {}^5I_8$ transition of Ho^{3+} around 893 nm appears after Yb^{3+} doping, which means the Yb^{3+} doping results in the population of $^5I_5$ state of Ho^{3+}. Interestingly, $^5I_5$ state of Ho^{3+} is precisely the intermediate level of the two-step ET process. Hence, the occurrence of $^5I_5 \rightarrow {}^5I_8$ transition of Ho^{3+} after Yb^{3+} doping is a strong evidence for the two-step ET process.

As depicted in Figure 7, with increasing Yb^{3+} concentration, the decay of $^5F_3$ level of Ho^{3+} rapidly speeds up, which can be explained by the existence of extra decay pathways due to the Yb^{3+} doping: ET from $^5F_3$ level of Ho^{3+} to Yb^{3+} increases the

DOI: 10.1021/acs.inorgchem.6b02600
Inorg. Chem. 2017, 56, 1498−1503

decay rate of Ho^{3+}: $^5F_3$ level. All the decay curves of the codoped samples exhibit nonexponential characteristics, resulting from the various ET rates from Ho^{3+} to Yb^{3+}. The lifetime values of the samples with different Yb^{3+} concentration are presented in Table 1, which are acquired from the integrating area of the corresponding normalized decay curves.

Table 1. Lifetimes and Energy Transfer Efficiencies η_{ETE} in Lu_2O_3: 1 mol % Ho^{3+}/x mol % Yb^{3+}

Yb^{3+} concentration (mol %)	lifetime	η_{ETE} (%)
0	73.2	0
1	70.1	4.2
5	62	15.3
10	49.4	32.5
20	33.8	53.8
30	27.8	62.0

The ET efficiency η_{ETE} can be calculated by

$$\eta_{ETE,Yb(x\%)} = 1 - \tau_{Yb(x\%)}/\tau_0 \quad (2)$$

where $\tau_{Yb(x\%)}$ represents the decay time of Ho^{3+}: $^5F_3$ level with various Yb^{3+} concentration, and τ_0 is the decay time of Ho^{3+}: $^5F_3$ level in Ho^{3+} single-doped sample. Utilizing the equation mentioned above, the η_{ETE} of each sample is obtained and listed in Table 1. Obviously, the η_{ETE} is improved from 4.2% to 62% with increasing Yb^{3+} doping concentration from 1 to 30 mol %.

CONCLUSIONS

In summary, an efficient NIR DC process has been verified in Lu_2O_3: Ho^{3+}/Yb^{3+} powder samples. Meanwhile, the DC mechanism from Ho^{3+} to Yb^{3+} has been explored in detail. On the basis of the analysis of Yb^{3+} doping concentration dependent on the initial transfer rate, we propose that the two-step ET process is the main way for ET from $^5F_3$ level of Ho^{3+} to $^2F_{5/2}$ level of Yb^{3+}. The ET efficiency reaches 62% for Lu_2O_3: 1% Ho^{3+}/30% Yb^{3+}. Unlike the common situations that the NIR photons are all emitted by the acceptors Yb^{3+}, the sensitizers Ho^{3+} also make contributions to the NIR emission upon 446 nm wavelength excitation. Beyond that, the $^5I_5 \rightarrow {}^5I_8$ transition and $^5F_4/{}^5S_2 \rightarrow {}^5I_6$ transition of Ho^{3+} as well as the $^2F_{5/2} \rightarrow {}^2F_{7/2}$ transition of Yb^{3+} match well with the optimal spectral response of crystalline silicon solar cells. Unfortunately, the strong $^5I_6 \rightarrow {}^5I_8$ transition of Ho^{3+} centered at 1208 nm is not suitable for the silicon solar cell to assimilate. However, it may have potential applications in the new wavelength laser oscillations and many other areas. The current experiment results indicate Lu_2O_3: Ho^{3+}/Yb^{3+} is a promising DC material for its application in solar cells.

AUTHOR INFORMATION

Corresponding Authors

*E-mail: zhangjh@ciomp.ac.cn. (J.Z.)
*E-mail: xianggt@cqupt.edu.cn. (G.X.)

ORCID

Guotao Xiang: 0000-0003-3587-6654

Notes

The authors declare no competing financial interest.

ACKNOWLEDGMENTS

This work is financially supported by National Key R&D Program of China (2016YFB0701003 and 2016YFB0400605), National Natural Science Foundation of China (61275055, 11274007, 51402284, 11604330, 11674044, 11404047, and 11604037), Natural Science Foundation of Jilin province (20140101169JC, 20150520022JH, and 20160520171JH), Chongqing Research Program of Basic Research and Frontier Technology (CSTC2015jcyjA50005, CSTC2016JCYJA0113, and CSTC2016jcyjA0207), and Scientific and Technological Research Program of Chongqing Municipal Education Commission (KJ1500409 and KJ1600406).

REFERENCES

(1) Dianov, E. M. Bismuth-doped optical fibers: a challenging active medium for near-IR lasers and optical amplifiers. *Light: Sci. Appl.* **2012**, *1*, e12.
(2) Qin, W. P.; Liu, Z. Y.; Sin, C. N.; Wu, C. F.; Qin, G. S.; Chen, Z.; Zheng, K. Z. Multi-ion cooperative processes in Yb^{3+} clusters. *Light: Sci. Appl.* **2014**, *3*, e193.
(3) Xiang, G. T.; Zhang, J. H.; Hao, Z. D.; Zhang, X.; Pan, G. H.; Luo, Y. S.; Lü, W.; Zhao, H. F. Importance of Suppression of Yb^{3+} De-Excitation to Upconversion Enhancement in β-$NaYF_4$: Yb^{3+}/Er^{3+}@β-$NaYF_4$ Sandwiched Structure Nanocrystals. *Inorg. Chem.* **2015**, *54*, 3921−3928.
(4) Stoneman, R. C.; Esterowitz, L. Efficient, broadly tunable, laser-pumped Tm:YAG and Tm:YSGG cw lasers. *Opt. Lett.* **1990**, *15*, 486−488.
(5) Wegh, R. T.; Donker, H.; Oskam, K. D.; Meijerink, A. Visible Quantum Cutting in $LiGdF_4$:Eu^{3+} Through Downconversion. *Science* **1999**, *283*, 663−666.
(6) Lee, T.; Luo, L.; Diau, E. W. G.; Chen, T. M.; Cheng, B. M.; Tung, C. Y. Visible quantum cutting through downconversion in green-emitting K_2GdF_5: Tb^{3+} Phosphors. *Appl. Phys. Lett.* **2006**, *89*, 131121.
(7) Li, J.; Chen, Li.; Hao, Z. D.; Zhang, X.; Zhang, L. G.; Luo, Y. S.; Zhang, J. H. Efficient Near-Infrared Downconversion and Energy Transfer Mechanism of Ce^{3+}/Yb^{3+} Codoped Calcium Scandate Phosphor. *Inorg. Chem.* **2015**, *54*, 4806−4810.
(8) Xiang, G. T.; Zhang, J. H.; Hao, Z. D.; Zhang, X.; Pan, G. H.; Luo, Y. S.; Lü, S. Z.; Zhao, H. F. The energy transfer mechanism in Pr^{3+} and Yb^{3+} codoped β-$NaLuF_4$ nanocrystals. *Phys. Chem. Chem. Phys.* **2014**, *16*, 9289−9293.
(9) Yu, K. H.; Chen, J. H. Enhancing Solar Cell Efficiencies through 1-D Nanostructures. *Nanoscale Res. Lett.* **2009**, *4*, 1−10.
(10) van der Ende, B. M.; Aarts, L.; Meijerink, A. Near-Infrared Quantum Cutting for Photovoltaics. *Adv. Mater.* **2009**, *21*, 3073−3077.
(11) van der Zwaan, B.; Rabl, A. P rospects for PV: a learning curve analysis. *Sol. Energy* **2003**, *74*, 19−31.
(12) Richards, B. S. Sol. Energy Mater. Enhancing the performance of silicon solar cells via the application of passive luminescence conversion layers. *Sol. Energy Mater. Sol. Cells* **2006**, *90*, 2329−2337.
(13) Strümpel, C.; McCann, M.; Beaucarne, G.; Arkhipov, V.; Slaoui, A.; Švrček, V.; del Cañizo, C.; Tobias, I. Modifying the solar spectrum to enhance silicon solar cell efficiency—An overview of available materials. *Sol. Energy Mater. Sol. Cells* **2007**, *91*, 238−249.
(14) Li, J.; Zhang, J. H.; Zhang, X.; Hao, Z. D.; Luo, Y. S. Cooperative downconversion and near infrared luminescence of Tm^{3+}/Yb^{3+} codoped Calcium Scandate phosphor. *J. Alloys Compd.* **2014**, *583*, 96−99.
(15) Trupke, T.; Green, M. A.; Würfel, P. Improving solar cell efficiencies by down-conversion of high-energy photons. *J. Appl. Phys.* **2002**, *92*, 1668−1674.
(16) Shockley, W.; Queisser, H. J. Detailed Balance Limit of Efficiency of p-n Junction Solar Cells. *J. Appl. Phys.* **1961**, *32*, 510−519.
(17) Li, Y.; Pan, Y. Influence of Yb^{3+} doping concentration on upconversion luminescence of Er^{3+} in Lu_2O_3 phosphor. *Optik* **2013**, *124*, 5131−5134.

DOI: 10.1021/acs.inorgchem.6b02600
Inorg. Chem. 2017, 56, 1498−1503

(18) Jiang, S.; Liu, J.; Lin, C. L.; Bai, L. G.; Xiao, W. S.; Zhang, Y. F.; Zhang, D. C.; Li, X. D.; Li, Y. C.; Tang, L. Y. Pressure-induced phase transition in cubic Lu_2O_3. *J. Appl. Phys.* **2010**, *108*, 083541.
(19) Li, R. M.; Gai, S. L.; Wang, L. Z.; Wang, J.; Yang, P. P. Facile synthesis and multicolor luminescent properties of uniform Lu_2O_3:Ln (Ln = Eu^{3+}, Tb^{3+}, Yb^{3+}/Er^{3+}, Yb^{3+}/Tm^{3+}, and Yb^{3+}/Ho^{3+}) nanospheres. *J. Colloid Interface Sci.* **2012**, *368*, 165−171.
(20) Xu, Q.; Lin, H.; Teng, H.; Chen, C.; Zhou, S. M. Energy transfer mechanisms of quantum cutting near infrared luminescence in Ho^{3+}/Yb^{3+} co-doped Y_2O_3 transparent ceramics. *J. Non-Cryst. Solids* **2014**, *403*, 84−87.
(21) Guo, L. N.; Wang, Y. H.; Zhang, J.; Wang, Y. Z.; Dong, P. Y. Near-infrared quantum cutting in Ho^{3+},Yb^{3+}-codoped $BaGdF_5$ nanoparticles via first and second-order energy transfers. *Nanoscale Res. Lett.* **2012**, *7*, 636.
(22) Zhou, X. J.; Wang, Y. J.; Zhao, X. Q.; Li, L.; Wang, Z. Q.; Li, Q. X. Near-Infrared Quantum Cutting via Downconversion Energy Transfers in Ho^{3+}/Yb^{3+} Codoped Tellurite Glass Ceramics. *J. Am. Ceram. Soc.* **2014**, *97*, 179−184.
(23) Dutta, P.; Rai, S. Optical transitions and frequency upconversions of Ho^{3+} and Ho^{3+}/Yb^{3+} ions in $Al(NO_3)_3$-SiO_2 sol-gel glasses. *Optik* **2011**, *122*, 858−863.
(24) Li, S. F.; Miao, Z.; Peng, Y.; Zhang, Q. Y. Optical properties and cooperative luminescence of Yb-doped borate-silicate glasses. *Chin. Phys. Soc.* **2006**, *55*, 4315−4320.
(25) Lin, H.; Chen, D. Q.; Yu, Y. L.; Yang, A. P.; Wang, Y. S. Near-infrared quantum cutting in Ho^{3+}/Yb^{3+} codoped nanostructured glass ceramic. *Opt. Lett.* **2011**, *36*, 876−878.

DOI: 10.1021/acs.inorgchem.6b02600
Inorg. Chem. 2017, 56, 1498−1503